Article

Length-Dependent Optical Effects in Single-Wall Carbon Nanotubes

Jeffrey A. Fagan, Jeffrey R. Simpson, Barry J. Bauer, Silvia H. De Paoli Lacerda, Matthew L. Becker, Jaehun Chun, Kalman B. Migler, Angela R. Hight Walker, and Erik K. Hobbie

J. Am. Chem. Soc., **2007**, 129 (34), 10607-10612• DOI: 10.1021/ja073115c • Publication Date (Web): 02 August 2007

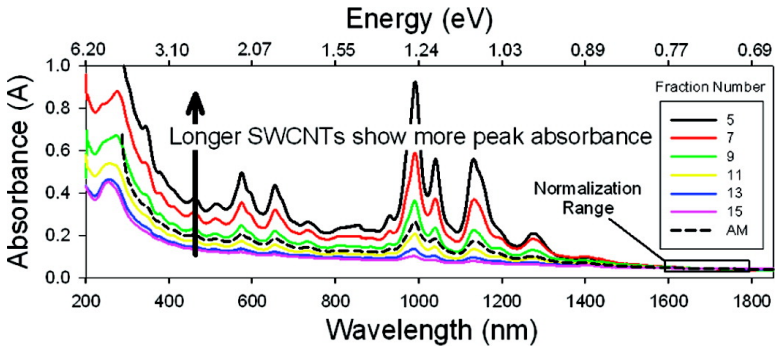

More About This Article

Additional resources and features associated with this article are available within the HTML version:

- Supporting Information
- Links to the 20 articles that cite this article, as of the time of this article download
- Access to high resolution figures
- Links to articles and content related to this article
- Copyright permission to reproduce figures and/or text from this article

View the Full Text HTML

J|A|C|S
ARTICLES
Published on Web 08/02/2007

Length-Dependent Optical Effects in Single-Wall Carbon Nanotubes

Jeffrey A. Fagan, Jeffrey R. Simpson, Barry J. Bauer, Silvia H. De Paoli Lacerda, Matthew L. Becker, Jaehun Chun, Kalman B. Migler, Angela R. Hight Walker,* and Erik K. Hobbie*

Contribution from the National Institute of Standards and Technology, Gaithersburg, Maryland 20899

Received May 16, 2007; E-mail: angela.hightwalker@nist.gov; erik.hobbie@nist.gov

Abstract: Among the novel chemical and physical attributes of single-wall carbon nanotubes (SWCNTs), the optical properties are perhaps the most compelling. Although much is known about how such characteristics depend on nanotube chirality and diameter, relatively little is known about how the optical response depends on length, the next most obvious and fundamental nanotube trait. We show here that the intrinsic optical response of single-wall carbon nanotubes exhibits a strong dependence on nanotube length, and we offer a simple explanation that relates this behavior to the localization of a bound exciton along the length of a nanotube. The results presented here suggest that, for a given volume fraction, the longest nanotubes display significantly enhanced absorption, near-infrared fluorescence, and Raman scattering, which has important practical implications for potential applications that seek to exploit the unique optical characteristics of SWCNTs.

Introduction

Highly touted as advanced materials, single-wall carbon nanotubes (SWCNTs) possess remarkable physical properties,[1] including very large tensile strength, high thermal and electrical conductivity, and well-defined optical absorption and fluorescence features that show a reproducible response to changes in the nanotube environment. Nonetheless, cost and quality remain major practical obstacles. The physical properties also vary with both the production method and the degree of nanotube dispersion, where the latter has been shown to have a significant impact on the SWCNT optical response.[2,3] Because of the relative transparency of biological materials in the near-infrared (NIR) region of the electromagnetic spectrum,[4] the NIR absorption and fluorescence of semiconducting SWCNTs, in particular, has generated substantial interest in the area of optical biological sensing[5−7] and optically activated therapeutics.[8] Applications that exploit these unique characteristics will undoubtedly demand well-dispersed and well-characterized materials, and recently developed processes that sort SWCNTs by both length and chiral vector[9−15] represent a major stride in this direction. These include ion-exchange chromatography[9,10] and density-gradient ultracentrifugation[11,12] to separate by band structure, as well as size-exclusion chromatography[9,13,14] and gel-permeation chromatography[15] to separate by length. Although much is known about how the SWCNT optical characteristics depend on nanotube chirality and diameter, relatively little is known about how such qualities depend on length, the next most obvious and fundamental nanotube trait.

In this contribution, we use size-exclusion chromatography to prepare length-separated fractions of individualized DNA-wrapped SWCNTs, which we then characterize using a combination of absorption, fluorescence, and resonant Raman spectroscopy. Robust changes in the peak versus baseline optical response are measured over a (10 to 700) nm range of nanotube lengths. Our compilation of data suggests that the intrinsic optical absorption of single-wall carbon nanotubes—the imaginary part of the dielectric response function of an isolated individual nanotube—increases nearly linearly with nanotube length, with no evidence of saturation up to length scales approaching 1 μm. As a possible explanation, we offer a simple physical argument that relates this length dependence to the

(1) Baughman, R. H.; Zakhidov, A. A.; de Heer, W. A. *Science* **2002**, *297*, 787.
(2) For example, see: Fagan, J. A.; Landi, B. J.; Mandelbaum, I.; Simpson, J. R.; Bajpai, V.; Bauer, B. J.; Migler, K.; Hight Walker, A. R.; Raffaelle, R.; Hobbie, E. K. *J. Phys. Chem. B* **2006**, *110*, 23801 and references therein.
(3) Crochet, J.; Clemens, M.; Hertel, T. *J. Am. Chem. Soc.* **2007**, *129*, 8058.
(4) For example, see: Wray, S.; Cope, M.; Delpy, D. T.; Wyatt, J. S; Reynolds, E. O. R. *Biochim. Biophys. Acta* **1988**, *933*, 184.
(5) Heller, D. A.; Jeng, E. S.; Yeung, T. K.; Martinez, B. M.; Moll, A. E.; Gastala, J. B.; Strano, M. S. *Science* **2006**, *311*, 508.
(6) Jeng, E. S.; Moll, A. E.; Roy, A. C.; Gastala, J. B.; Strano, M. S. *Nano Lett.* **2006**, *6*, 371.
(7) Cherukuri, P.; Bachilo, S. M.; Litovsky, S. H.; Weisman, R. B. *J. Am. Chem. Soc.* **2004**, *126*, 15638.
(8) Kam, N. W.; O'Connell, M.; Wisdom, J. A.; Dai, H. *Proc. Natl. Acad. Sci. U.S.A.* **2005**, *102*, 11600.
(9) Zheng, M.; Jagota, A.; Semke, E. D.; Diner, B. A.; McLean, R. S.; Lustig, S. R.; Richardson, R. E.; Tassi, N. G. *Nat. Mater.* **2003**, *2*, 338.
(10) Huang, X. Y.; McLean, R. S.; Zheng, M. *Anal. Chem.* **2005**, *77*, 6225.
(11) Arnold, M. S.; Stupp, S. I.; Hersam, M. C. *Nano Lett.* **2005**, *5*, 713.
(12) Arnold, M. S.; Green, A. A.; Hulvat, J. F.; Stupp, S. I.; Hersam, M. C. *Nat. Nanotechnol.* **2006**, *1*, 60.
(13) Niyogi, S.; Hamon, M. A.; Bhowmik, P.; Rozenzhak, S. M.; Itkis, M. E.; Meier, M. S.; Haddon, R. C. *J. Am. Chem. Soc.* **2001**, *123*, 733.
(14) Bauer, B. J.; Becker, M. L.; Bajpai, V.; Fagan, J. A.; Hobbie, E. K.; Migler, K.; Guttman, C. M.; Blair, W. R. *J. Phys. Chem. C* **2007**, JP071494Q ASAP.
(15) Heller, D. A.; Mayrhofer, R. M.; Baik, S.; Grinkova, Y. V.; Usrey, M. L.; Strano, M. S. *J. Am. Chem. Soc.* **2004**, *126*, 14567.

localization of a bound exciton along the backbone of the nanotube, suggesting a quantitative link between nanotube length and oscillator strength for quasi-1D ordered nanostructures. Our results suggest that the longest SWCNTs display the strongest optical features, which has profound implications for all potential applications that seek to exploit the unique optical characteristics of single-wall carbon nanotubes.

Materials and Methods

The measurements presented here were performed on SWCNTs grown through the cobalt-molybdenum-catalyst (CoMoCat) process, but analogous behavior was also measured for SWCNTs grown with the high-pressure carbon monoxide (HiPCO) process, laser ablation, and electric arc methods. Aqueous dispersions of CoMoCat SWCNTs (Southwest Nanotechnologies Inc. Batch NI-6-A001 S-P95-02), HiPCO SWCNTs (CNI Batch 0286), laser ablation SWCNTs (NASA/JSC purified soft-bake SWCNTs), and electric arc SWCNTs (Carbolux) were achieved following the method of Zheng et al.[9] by sonication in an ice water bath (10 W, 3.2 mm tip sonicator) of 1 mg/mL nanotubes in salt solution (0.2 mol/L NaCl, 0.04 mol/L Tris, HCl to pH = 7.0) in the presence of 1 mg/mL 30-mer 5′-GT$(GT)_{13}$GT-3′ single-stranded DNA (Integrated DNA Technologies) for 2 h, followed by centrifugation (2 h, 21 000 g). The supernatant was a stable black liquid containing well dispersed individual nanotubes. SEC was performed using an Agilent 1200 pump with a SepaxCNT (SEC-2000 + SEC-1000 + SEC-300) column set. Centrifuged samples were filtered through a 0.45 μm filter and injected in 0.5 mL increments with a 0.5 mL/min flow rate. Fractions (25) were collected at 2 min intervals, with the first (longest) nanotubes in fraction 5 and progressively shorter nanotubes in following fractions. After fraction 16, the apparent SWCNT concentration rapidly decreases, and free DNA elutes in fractions 17 through 19. Repetitions (18) of the chromatographic separation were performed for the CoMoCat SWCNTs, 5 for the HiPCO and electric arc SWCNTs, and 1 for the laser SWCNTs; for each synthesis method the corresponding fractions were combined and concentrated by forced dialysis across a 30 kD nominal cutoff membrane to concentrations of up to approximately 0.5 mg/mL. For all runs of chromatographic separation, a UV−vis photodiode array (Waters 2996) and a Multiple Angle Light Scattering (MALS) instrument (Wyatt Dawn EOS multi-angle light scattering detector) were used to record the absorbance (250−800 nm) and light scattering (filtered to remove fluorescence contributions) as a function of time. The MALS data were fit, and the mean nanotube length of each fraction was extracted using established theoretical expressions for classical scattering from a rigid rod.

In addition to MALS, length characterization was also performed using dynamic light scattering (DLS), atomic force microscopy (AFM), and transmission electron microscopy (TEM). For AFM measurements, the nanotube dispersions were further processed either by dialysis of the aqueous ssDNA/SWCNT suspensions across a 50 000 relative molecular mass membrane (Spectra-Por) or through forced dialysis against a 30 000 relative molecular mass ultrafiltration membrane (Millipore), against/with 18+ MΩ distilled deionized water to reduce the salt content. Solutions were subsequently diluted with 18+ MΩ water to reduce nanotube density prior to deposition on the surface. Freshly cleaved mica surfaces were dipped into the dialyzed solutions for 5 s, rinsed with distilled deionized water, and finally dried in an oven at 50 °C. Images of the nanotubes on the prepared surfaces were obtained in air using a Digital Instruments NanoScope IV with standard silicon tips (nominal spring constant 40 N/m); on the order of 100 nanotubes were measured for each of the fractions 5 through 11. The additional time required to find and image smaller nanotubes limits the usefulness of AFM imaging for fractions above 11. DLS was performed in a temperature-controlled cell maintained at 25 °C using a Brookhaven Instruments BI-200SM in a crossed polarizer configuration with excitation at 488 nm from an argon ion (Ar+) laser.[16] Scattering was measured at a minimum of five different angles for each fraction. The correlation function in each case was fit with a double exponential relaxation, and the rotational relaxation time was obtained using established theoretical procedures by extrapolating the decay rate of the faster relaxation rate to the zero scattering angle.[16] Lengths were then calculated from the measured rotational relaxation times using the established theoretical expression for the orientational diffusivity of a thin rigid rod.[16] TEM samples were prepared by placing a drop of diluted dialyzed nanotube suspension onto a carbon-coated TEM grid and freeze-drying. TEM measurements were performed on a Philips EM400T. Lengths reported in this contribution are an average of the AFM and DLS data, which we identify as the two most robust and precise metrics of nanotube length in the present study. These measurements are consistent, however, with lengths suggested by the TEM images and the R_g extracted from MALS using a fit of polydisperse rods to the measured scattering data. Fraction length as a function of fraction number is detailed in Figure 1. Since the latter maps linearly onto elution time, an exponential decay in nanotube length, L, reflects a residence time in the porous column that scales inversely with L. Throughout the paper, error bars are the size of the data points, unless otherwise indicated, and represent two standard deviations in the total experimental uncertainty.

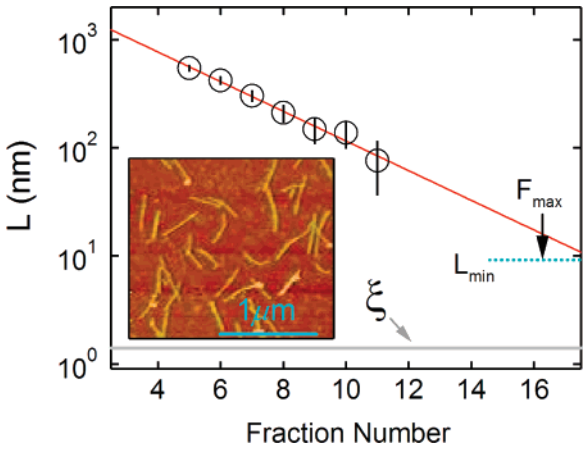

Figure 1. Mean SWCNT length as deduced from a combination of DLS and AFM as a function of fraction number with an exponential fit, where the inset shows an AFM image of fraction 6. The approximate localization length (ξ) of an 11 bound exciton is also indicated.

Ultraviolet (UV)−visible (vis)−near-infrared (NIR) absorption spectroscopy was performed in transmission mode on a Perkin-Elmer Lambda 950 UV−vis−NIR spectrophotometer over the range 185−1880 nm. In all experiments, the incident light was circularly polarized, and the instrument was corrected for both the dark current and background spectra. The reference beam was left unobstructed during the measurement, with the subtraction of the appropriate reference sample performed during data reduction. Absorption spectra were recorded at 1 nm increments, with an instrument integration time of 0.2 s per increment, using a 1, 2, or 10 mm quartz cuvette, depending upon the magnitude of the extinction for a particular sample. To check for the effects of scattering, an integrating sphere detector was also used for some of the samples. No significant changes in the measured absorption were seen in the UV−visible section of the spectrum in these instances; in the NIR region, small decreases in absorption were observed at the optical transitions, but these are likely related to the spurious detection of SWCNT fluorescence.

Fluorescence characterization was performed on a JY-Horiba nanolog-3 spectrofluorometer with a liquid nitrogen cooled InGaAs detector. Emission spectra are corrected for the instrument's source spectral distribution, detector spectral response, and the absorbance of

(16) Supporting Information Online.

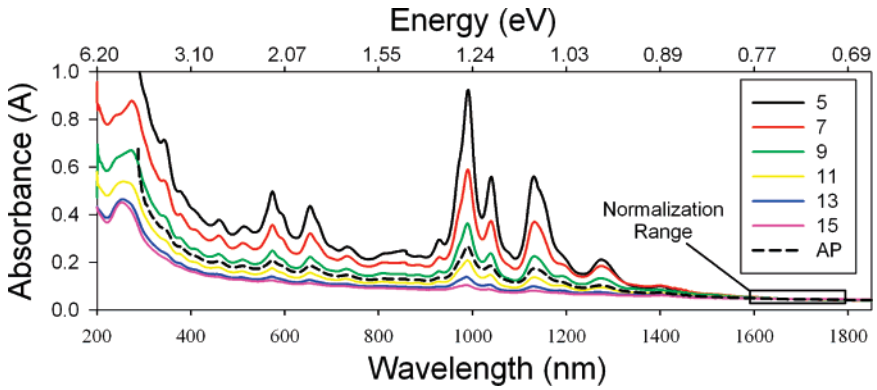

Figure 2. Optical absorption spectra for different L, where the dominant peak near 1.2 eV corresponds to the E_{11}^S transition of a (6,5) SWCNT.

the filter used to restrict the scattered excitation light from the NIR monochromotors and detector. The excitation wavelength was scanned in 5 nm increments using a 450 W xenon lamp through a 10 nm slit with emission collected at 90° in 1, 2, or 4 nm increments through a 10 nm slit. To account for differences in concentration, fractions were diluted to a common extinction of 0.15 cm^{-1} at 775 nm and were measured in a 10 mm path length quartz cuvette.

Resonance Raman spectra were collected in a collinear backscattering configuration. A Ti:Sapphire ring laser (Coherent 899 Ring Laser) pumped by an Ar+ laser (Coherent Innova Sabre with multi-line visible head), and the Ar+ laser by itself, provided a tunable pump source at approximately 10 to 25 mW of power focused to a spot size of approximately 100 μm. Samples were measured in a single semi-micro spectrophotometer cell (NSG, 10 mm path length) that was held immobile for all of the measurements. The spontaneous Raman backscattered light was collected with a triple grating spectrometer (f/# = 6 aperture, Dilor XY800) and a liquid nitrogen cooled CCD detector. The signal was integrated for an appropriate time to obtain a signal-to-noise ratio greater than 50. A typical integration time for the CoMoCat fractions was 60 to 90 s averaged over four scans. Data were collected at discrete excitation wavelengths with the Ar+ laser alone, 457.9, 488.0, 501.7, and 514.5 nm, and for multiple wavelengths within the range of the Ti:Sapphire laser. In the 690 to 850 nm range of the Ti:Sapphire laser, measurements were performed at the resonant excitation energies for several SWCNTs. At the 514.5 nm excitation line, Raman frequency shifts in the range 150 to 4400 cm^{-1} were measured, with specific attention given to those between 150 and 2800 cm^{-1}. To control for variations in signal, a serial dilution experiment of concentrated SWCNTs was performed, and the intensity of the Raman signal for a given material was found to plateau above a threshold concentration. Measurements on the size fractions were then performed on samples concentrated above this threshold. Data were corrected solely by scaling for incident laser intensity and by the subtraction of a small linear background, generally less than a few percent of the feature intensity. This point is discussed further in the on-line Supporting Information.[16]

Results and Discussion

The absorption data in Figure 2 show a clear dependence on L, with all of the interband optical transitions increasing (relative to the baseline π-plasmon absorbance) with nanotube length. The increase in the peak absorption relative to the baseline is clearly seen for E_{11}^S (850−1450 nm) and E_{22}^S (500−850 nm), although such trends are less quantitative for E_{11}^M (420−520 nm) and E_{33}^S (340−400 nm). No measurable shifts in the energy of the optical transitions are observed. The low SWCNT concentration of the respective fractions has, to this point, precluded an absolute determination of nanotube concentration in each fraction via direct weighing. To account for the variations in SWCNT concentration, i.e., volume fraction, with the collected fraction number, the data have thus been normalized by the absorption in the long-wavelength limit. We have discounted potential artifacts such as the presence of non-SWCNT carbon impurities and variations in SWCNT concentration; such effects are negligible[16] in comparison to the trends shown in Figure 2. We note that the interpretation offered here was likely suppressed in a previous study due to the choice of normalization.[9] Each SWCNT is characterized[17] by a chiralty vector (n, m) that describes how the 2D graphene sheet rolls into a tube of diameter a. In assessing the influence of nanotube length on optical absorption, we focus on the (6, 5) SWCNT, which for aqueous DNA-wrapped dispersions has its first interband transition in the vicinity of $\lambda = 990$ nm. At this excitation, the range of SWCNT lengths (10 nm $< L <$ 700 nm) is in the Rayleigh regime $L < \lambda/n$, where n is the refractive index of the suspending medium.[16] For the low concentrations of interest here, extinction due to scattering is negligible, and classical arguments alone cannot account for the observed variation with nanotube length.[16]

As noted above, scaling of the absorbance spectra in Figure 2 to correct for variations in nanotube concentration with fraction number was performed in the long-wavelength limit, as the underlying background absorption is expected to vary smoothly at energies below the optical transitions of the SWCNTs. In the choice of different locations for scaling, it is difficult to find a wavelength regime other than the long wavelength limit where there are limited contributions from any interband transition or graphitic carbon features. Scaling the data so that the peak intensities coincide requires the *a priori* assumption that there is no length dependence in the optical response, which we believe is unjustified.[16] We emphasize, however, that scaling the data at other nonpeak locations such as the π-plasmon or in between the first and second interband transitions, such as at 775 nm, *does not change the order of magnitude of the observed length dependence*. The dependence of the (6,5) E_{11}^S absorption peak on SWCNT length is shown in Figure 5A, which reveals an overall approximately linear trend, regardless of the normalization scheme used. Lengths below 80 nm in Figure 5 have been extrapolated from the fit shown in Figure 1.

As might be expected, the length-dependent absorption leads to an analogous variation in the fluorescence intensity, as previously suggested by Heller et al.[15] for SWCNTs dispersed

(17) Dresselhaus, M. S.; Dresselhaus, G.; Avouris, P. *Carbon Nanotubes: Synthesis, Structure, Properties, and Applications*; Springer-Verlag: Heidelberg, 2001.

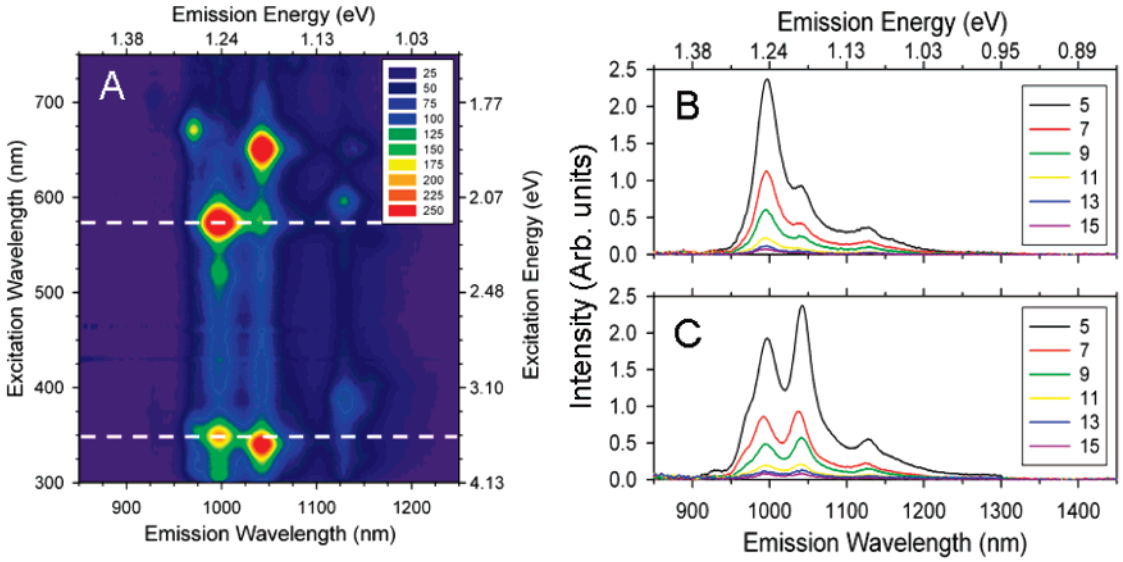

Figure 3. (A) Fluorescence intensity map of fraction 5, focusing on the E_{22}^S and E_{33}^S transitions of the (6,5) and (7,5) SWCNT. (B) Fluorescence spectra for different length fractions at 572 nm excitation for the (6,5) feature from the 2D plot in (A). (C) Fluorescence spectra for different length fractions at 344 nm excitation for the (6,5) feature from the 2D plot in (A).

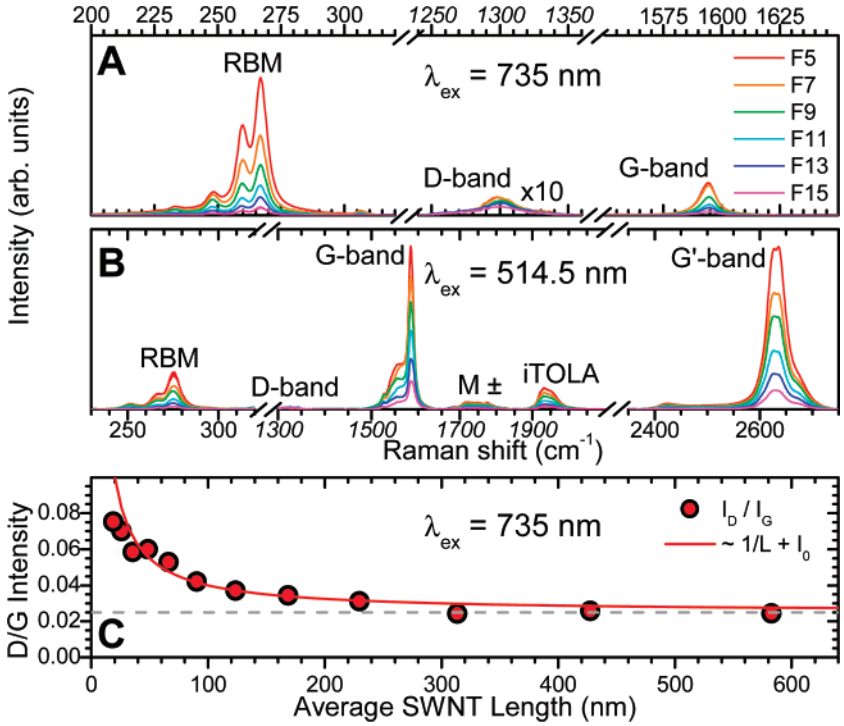

Figure 4. (A) Length-dependent Raman scattering at 735 nm excitation from the resonant radial breathing mode (RBM) of a minority SWCNT, as well as the D-band (×10) and G-band for the same excitation. (B) At 514 nm excitation, no RBM is resonant and the G-band scattering appears large. Additional length-dependent features (M±, iTOLA) were measured at this excitation, including the nondispersive G′ peak at 2450 cm^{-1}. (C) At both excitations, the strength of the G-band with respect to the D-band is indicative of relatively high sample quality.

with sodium dodecylsulfate (SDS) and length sorted by electrophoretic gel migration. Figure 3A displays a wide excitation scan of the fractionated CoMoCat material along with the resulting emission profile. The length dependence of the fluorescence is seen in Figure 3B and C, which show the fluorescence spectra for the slices denoted in Figure 3A for each fraction. Excitation at either the second or third interband transition produces spectra with similar length dependences, although the background π-plasmon absorption is vastly different at the two locations. Shorter nanotubes display smaller peak absorption with respect to any impurity or π-plasmon feature, and this ratio is much smaller at the third interband transition than at the second. In either case, the length dependence is again approximately linear, as shown in Figure 5A.

Raman scattering (Figure 4) displays a multitude of spectral features in response to laser excitation. Both resonant and nonresonant modes are observed, including the SWCNT-specific radial breathing mode (RBM), $M^{+,-}$, and iTOLA modes, as well as the D, G, and G′ bands common to graphitic materials. The strength of each of the SWCNT specific modes as well as the G and G′ modes are observed to increase significantly with

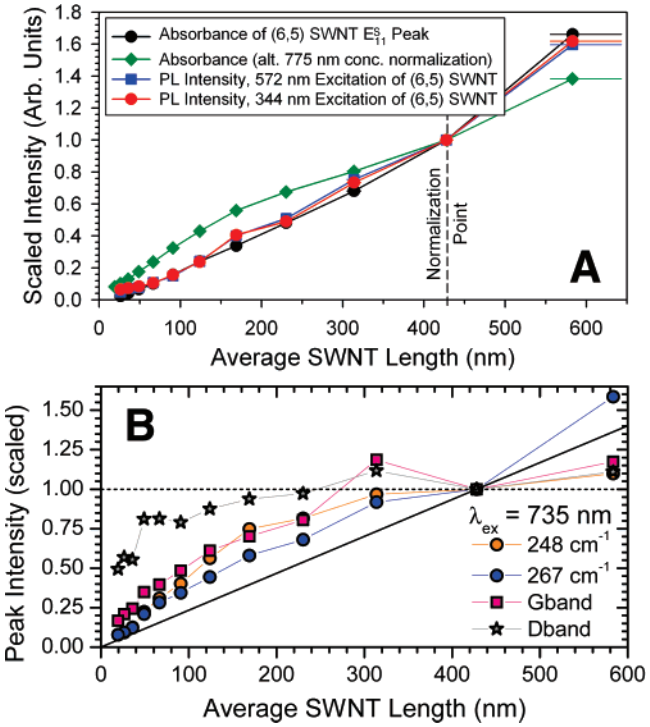

Figure 5. (A) Length dependence of the absorption and fluorescence features in Figures 2 and 3. The black symbols are the E_{11}^S absorption of the (6,5) SWCNT, open squares are the fluorescence from the 572 nm excitation of the (6,5) SWCNT, and the red symbols are from 344 nm excitation of the (6,5) SWCNT. Also shown in green is the result obtained using the 775 nm valley as the point of reference for the normalization of concentration variations with fraction number. (B) Length dependence of Raman scattering (735 nm excitation) for different Raman frequencies. In (A), error bars in L denote the range of values measured for the average length of specific fractions by the different characterization methods.

SWCNT length, whereas the D band, associated with defect density, shows a weaker response to such changes. Although the exact relative weights of the different bands change with excitation wavelength, by a measure of the D/G ratio (which is less than 0.016 for fraction 5 at $\lambda = 514$ nm), the longest fractions considered here represent high quality materials.[16] The D/G ratio as a function of nanotube length is shown in Figure 4C, along with a fit of the data to a $1/L$ functional form, the expected dependence when considering the end caps as defects. This is consistent with another recently reported study of the effect of SWCNT length on resonant Raman scattering.[18] Shape scattering from a nonabsorbing rod is expected to scale linearly[16] with L, but the Raman scattering intensities, shown in Figure 5B, are clearly nonlinear in length. Qualitatively, we would expect the length-dependent extinction depicted in Figure 2 to influence the scattering from a resonant Raman feature, albeit in a complicated fashion for the scattering geometry in question, and we heuristically attribute the curvature in Figure 5B to such absorption effects.

The empirical results offered here raise intriguing questions about the nature of the optical excitations in SWCNTs that might implicate any one or a combination of factors, including the size and mobility of excitons, as well as the distribution and influence of defects and impurities in nanotubes of varying length. The results we present here will hopefully serve as a guide to detailed computational and theoretical efforts, as well as further experimental studies focused on the question of length dependent optical effects, and here we can only speculate as to the possible origins. In a general sense, the phenomena reported here bear a striking resemblance to the behavior exhibited by broad class of ordered molecular aggregates,[19] and we draw on this formalism in our discussion. On a microscopic level, optical absorption is the product of nanotube volume fraction and the imaginary part of the intrinsic SWCNT optical response. As noted above, the data in Figure 2 are presumed to be normalized by nanotube volume fraction, so changes with L are believed to reflect changes in the imaginary part of the intrinsic SWCNT dielectric response function,

$$\epsilon''(\omega) \propto \sum_S |\langle S|\hat{\mu}|0\rangle|^2 \, \delta(\hbar\omega - E_S) \qquad (1)$$

where $\hat{\mu}$ is the transition dipole moment operator, $|S\rangle$ denotes the normalized optically excited state of energy E_S, and $\langle S|\hat{\mu}|0\rangle$ is the optical transition matrix element.[20,21] Focusing on the E_{11}^S transition, which provides the most definitive length-dependent signal in the present study, a bound exciton is thought to be localized on a scale[20−23] of $\xi \approx 1$ nm along the length of the nanotube, which we model as a linear chain of $N = L/\xi$ segments along a coordinate z. The normalized state of a bound exciton located at segment n is denoted $|n\rangle$, with a wave function $\psi_n(z) = \langle z|n\rangle$. If the excitation is an incoherent superposition of the N different localized states, then the matrix element in eq 1 is that of a single bound exciton, $\langle n|\hat{\mu}|0\rangle = \mu_s$, and the sum in eq 1 could in principle just scale as the number of available sites, $N \propto L$. Another much more intriguing possibility, however, is a coherent superposition of the N localized elements,

$$|S\rangle = (1/\sqrt{N}) \sum_{n=1}^{N} e^{ikn}|n\rangle \qquad (2)$$

where k is an integer multiple of $2\pi/N$. Note that $|S\rangle$ still has the same energy as $|n\rangle$, but the wave function

$$\langle z|S\rangle = (1/\sqrt{N}) \sum_{n=1}^{N} e^{ikn} \psi_n(z) \qquad (3)$$

now exhibits phase coherence along the nanotube. The transition matrix element then becomes

$$\langle S|\hat{\mu}|0\rangle = (1/\sqrt{N}) \sum_{n=1}^{N} e^{ikn}\langle n|\hat{\mu}|0\rangle = \sqrt{N}\mu_s\delta_{k,0} \qquad (4)$$

with the sum in eq 1 again scaling as N. Although oscillator strength alone might not be the most definitive way to distinguish between these two possible scenarios, one could argue that a degree of coherence in the excitation—reflecting the fact that L is significantly larger than the Bohr radius of the lowest energy bound exciton but still smaller than λ—might be expected, based on the relatively clean 2D crystal structure of

(18) Chou, S. G.; Son, H.; Kong, J.; Jorio, A.; Saito, R.; Zheng, M.; Dresselhaus, G.; Dresselhaus, M. S. *Appl. Phys. Lett.* **2007**, *90*, 131109.
(19) Hanamura, E. *Phys. Rev. B* **1998**, *37*, 1273.
(20) Perebeinos, V.; Tersoff, J.; Avouris, P. *Phys. Rev. Lett.* **2004**, *92*, 257402.
(21) Spataru, C. D.; Ismail-Beigi, S.; Capaz, R. B.; Louie, S. G. *Phys. Rev. Lett.* **2004**, *92*, 077402.
(22) Araujo, P. T.; Doorn, S. K.; Kilina, S.; Tretiak, S.; Einarsson, E.; Maruyama, S.; Chacham, H.; Pimenta, M. A.; Jori, A. *Phys. Rev. Lett.* **2007**, *98*, 067401.
(23) Wang, F.; Dukovic, G.; Brus, L. E.; Heinz, T. F. *Science* **2005**, *308*, 838.

graphene.[17] Measurements of the nonlinear optical susceptibility and the decay rate of the NIR fluorescent state as a function of SWCNT length would be quite revealing in this regard. Our measurements are not sensitive enough to provide quantitative information about the length dependence of the strength of the higher-order E_{33}^S and E_{44}^S transitions, which are thought to be weakly localized or even delocalized,[21,22] but one could argue that a dependence on SWCNT length might be expected for any excitation that extends over the length of the nanotube.

Conclusions

The intrinsic optical response of single wall carbon nanotubes, i.e., the optical absorption and fluorescent emission at constant nanotube volume fraction, is shown to have an approximately linear dependence on nanotube length. The peak versus baseline absorbance at optical resonance is found to scale almost linearly with nanotube length up to length scales approaching 1 μm. This size dependence directly impacts both the NIR fluorescence and the resonant Raman scattering features exhibited by the SWCNTs. The implications of this additional factor of L in the absorption can perhaps be qualitatively understood in simple semiclassical and heuristic terms. In the Rayleigh regime, the optical extinction is the product of the number of nanotubes per unit volume and the optical absorption cross section of a single nanotube, where the latter scales as the SWCNT cross-sectional area, aL, times the imaginary part of the SWCNT dielectric response function, $\epsilon''(\omega)$. Nanotube volume and cross-sectional area both scale as L, and at constant nanotube volume fraction any leftover length dependence must therefore reside in $\epsilon''(\omega)$. In a purely classical picture, the length scale of the excitation, λ, is larger than L and $\epsilon''(\omega)$ is intuitively a constant independent of L. In the more correct quantum picture, however, the bound exciton is localized on a length scale much smaller than the length of the nanotube or λ, implying that $\epsilon''(\omega)$ is proportional to L. Although our data show no sign of saturation for the longest nanotubes considered here, we would not expect this trend to continue unbounded, regardless of the nature of the excitation. Defects, kinks, impurities, and tube deformation are all potential factors that could ultimately put limits on the length dependence.

These results presented have substantial implications for the evaluation of mixed SWCNT materials through optical means, as well as the selection of material for potential applications. For example, the choice of SWCNTs as microscale optical sensors or as *in vivo* probes of local chemical environment is directly impacted by this work. For other applications, such as in targeted chemotherapeutics, the desire to increase optical properties will need to be weighed against the limited cellular uptake[24] of high-aspect-ratio SWCNTs.

Acknowledgment. The authors thank M. Dresselhaus, M. Strano, B. Weissman, B. Hauge, M. Zheng, J. Kuno, L. Richter, T. Heinz, and G. Bryant for useful discussions, as well as T. Chastek for contributing to the supporting online information.

Supporting Information Available: An analysis of impurity effects and a more detailed discussion of the optical measurements, including background and references, can be found in the Supporting Information online. This material is available free of charge via the Internet at http://pubs.acs.org.

JA073115C

(24) Becker, M. L.; Fagan, J. A.; Gallant, N. D.; Bauer, B. J.; Bajpai, V.; Hobbie, E. K.; Lacerda, S. H.; Migler, K. B. and Jakupciak, J. P. *Adv. Mater.* **2007**, *19*, 939.